6.1 Introduction

Materials that give responses to various external stimuli gained much interest due to their intriguing rich physics and prospect for technological device applications [1-3]. Particularly, the class of oxide double perovskites (DP) $A_2BB'O_6$ (A= Rare earth ions or alkaline ions; B/B'= transition metal ions)[4] has attracted a great deal of research attention due to their diverse exotic properties *viz*. giant magneto-resistance, spin reorientation, magnetocaloric effects, colossal magneto-dilectric effect, E-type (↑↑↓↓) of ordering driven ferroelectricity, metamagnetic transition, anti-site disorder driven multi-glass phases, giant exchange bias, Griffiths phase [5-14] etc. Hence, these complex and interesting physical properties can be harnessed to fabricate innovative devices for practical applications. Apart from the technological prospects, it also offered a fascinating and broad playground for basic condensed matter research viz., strong cooperative effects among different micro-structural degrees of freedom, such as spin, structural disorder, phonon, orbital momentum and charge etc. For DPs, the strong interplay of B-site disorder and its spins has profound effects on its physical properties, particularly on its magnetic properties [10-11,15-19]. It has been observed that competing ferromagnetic (FM) and anti-ferromagnetic (AFM) interactions (raised by B-site disorder) are the basic ingredients in anticipating emergence of short range ordering related secondary magnetic phases like low temperature Griffiths phase (GP), spin-glass, exchange bias etc [8-14].

As a matter of fact, FM system was initially thought to be a prerequisite for exhibition of GP [13-14, 20-24]. However, recently, GP has been reported in very few AFM systems viz., Ca_3CoMnO_6, $R_{0.5}Eu_{0.5}MnO_3$, $GdFe_{0.17}Sn_2$ systems where the existence of GP has been explained by means of small sized FM clusters [24-26]. Moreover, in a very recent report, another geometrically frustrated AFM system $DyBaCo_4O_{7+\delta}$ was found to exhibit GP

behaviour where the short-range correlations arise due to the interactions of Co^{2+}/Co^{3+}ions [27].

On the other hand, when long range magnetic ordering of a system gets frustrated due to increasing competing FM/AFM interactions on cooling the temperature, it re-enters in a glassy state, called re-entrant spin glass (RSG) or cluster glass (RCG) state [11,28-30]. This particular dynamic magnetic property has attracted immense research interest world-wide over last few decades for understanding its intriguing physics and scopes for practical applications [28-32]. Eventually, as compared to the large number of systems exhibiting spin-glass states, fewer systems are reported to show RSG or RCG states such as FM La_2NiMnO_6, Lu_2MnNiO_6, Kagome ferrite $SrSn_2Fe_4O_{11}$, spiral magnet $BiMnFe_2O_6$ etc. [11,28-32]. The different theoretical and experimental investigations showed different possible mechanisms are associated to the observed glassiness viz., site disorder, geometrical spin frustration, spin-orbit interaction, octahedral tilting etc [28-34]. However, the exact origin is still an open challenge and requires more efforts to be addressed.

In contrast to the widely studied ordered $A_2BB'O_6$ (B/B'=Mn, Co, Ni) compounds, the studies on the Fe based DPs i.e. R_2BFeO_6 oxides (where B-site disorder is inevitable), are comparatively limited and thus there are much more opportunities to explore their properties [6, 35-37]. In our previous chapter, we have investigated the electronic structure and revealed the existence of strong spin-phonon coupling for at least two phonon modes in such a B-site disordered DP Pr_2CoFeO_6 (PCFO). In the present chapter, we shall mainly focus on investigating its magnetic properties with the aim of giving a comprehensive study of the role of B-site disorder and Co/Fe interactions in deciding its magnetic ground state. Here, the one end member $PrFeO_3$ is a canted AFM insulator [38]. Eventually, the orthoferrites $RFeO_3$ are known for their extraordinary properties viz., spin-reorientation transitions, existence of Bloch line, magnetization reversal, and high domain wall velocity etc. which found

applications in magneto-optical, bubble memory etc data storage devices [38-41]. On the other hand, cobaltites $RCoO_3$, are well-known systems since 1950s and particular attention has been given to the thermally driven spin state transition from the low spin LS (t_{2g}^6) state to the higher spin states of the Co^{3+} ions [42-46]. In particular for $PrCoO_3$, it is controversial whether the spin state of Co^{3+} remains in LS or in higher states (IS or HS) upto 300 K [45-46]. In our earlier chapter, however, we have shown that Co^{3+} in PCFO exists in low spin state. Thus, understanding the above facts, PCFO is expected to possess an assorted magnetic, electrical and structural properties depending highly on the spin states of the Co/Fe, structural disorder and the modified spin interactions in the system.

In this chapter, we have presented temperature dependent (DC and AC) magnetization, and Neutron diffraction study of PCFO. We have also performed its *ab* initio band structure (DFT) calculations for investigating its electronic and magnetic properties.

6.2 Experimental details

6.2.1 Sample synthesis:

The detailed procedures for the sample preparation of the present system PCFO has been already discussed in the previous chapter.

6.2.2 Characterizations:

The neutron diffraction measurements were carried out on the PD2 neutron powder diffractometer (λ =1.2443 A°) at the Dhruva reactor in Bhaba Atomic Research Centre, Mumbai, India. The superconducting quantum interference device (SQUID) based magnetic property measurement system (Quantum Design-MPMS) was employed for magnetization measurements.

6.3 Computational details:

We have performed our study based on density functional theory (DFT) using Vienna *ab* initio simulation package (VASP). Exchange-correlation potential (Perdew-Burke-Ernzerhof exchange-correlation functional) is approximated with generalized gradient approximation (GGA). The projector augmented wave method (PAW) is used for core-valence interaction. The calculations were performed with K-mesh of 8×5×8 for Pr_2CoFeO_6 with Pnma space group. We have considered plane-wave basis up to cut-off energy 600 eV for convergence. The lattice parameters are optimized before the calculation of DOS to reduce internal forces. To see the spin polarized partial and total DOS, we have considered the on-site coulomb correction (GGA+U).

6.4 Results and discussions

6.4.1 Density of states study by ab initio calculations:

We have performed the ab initio calculations based on density function theory (DFT) for PCFO to get more insights into its electronic and magnetic structures. The structure has been optimized with orthorhombic Pnma symmetry. The structure was relaxed till the Feynman-Hellman forces were reduced below 0.001 eV $(A^0)^{-1}$. The optimized structure reached to the lowest energy of ~ -154.421 eV.

This optimized structure has been used to calculate the density of states (DOS). All the DOS calculations have been carried out with generalized gradient approximation (GGA) scheme for the exchange correlation potential (i.e. using GGA+U approximation). The calculations have been done with Hubbard U correction i.e.U_{eff}=U-J (here J and U are exchange and Coulomb parameters respectively) which are considered to be ~3 eV for Pr-*4f*

states [47], ~3 eV for Co-*3d* states [48] and ~4 eV for Fe-*3d* states [49]. We have performed our calculations both for FM and AFM couplings among spins. However, the calculations yielded that the structure with AFM coupling among spins are energetically favourable than for FM couplings. Hence, the calculation predicts an AFM ground state for the present PCFO system. We have calculated the total density of states (TDOS) for PCFO system which shows absence of density of states near Fermi level, suggesting the insulating nature of the system which corroborates our previous work by XPS study (Fig. 6.1 (a)). Interestingly, the resistivity measurement of PCFO at room temperature showed a value of ~886 Ohm-m which

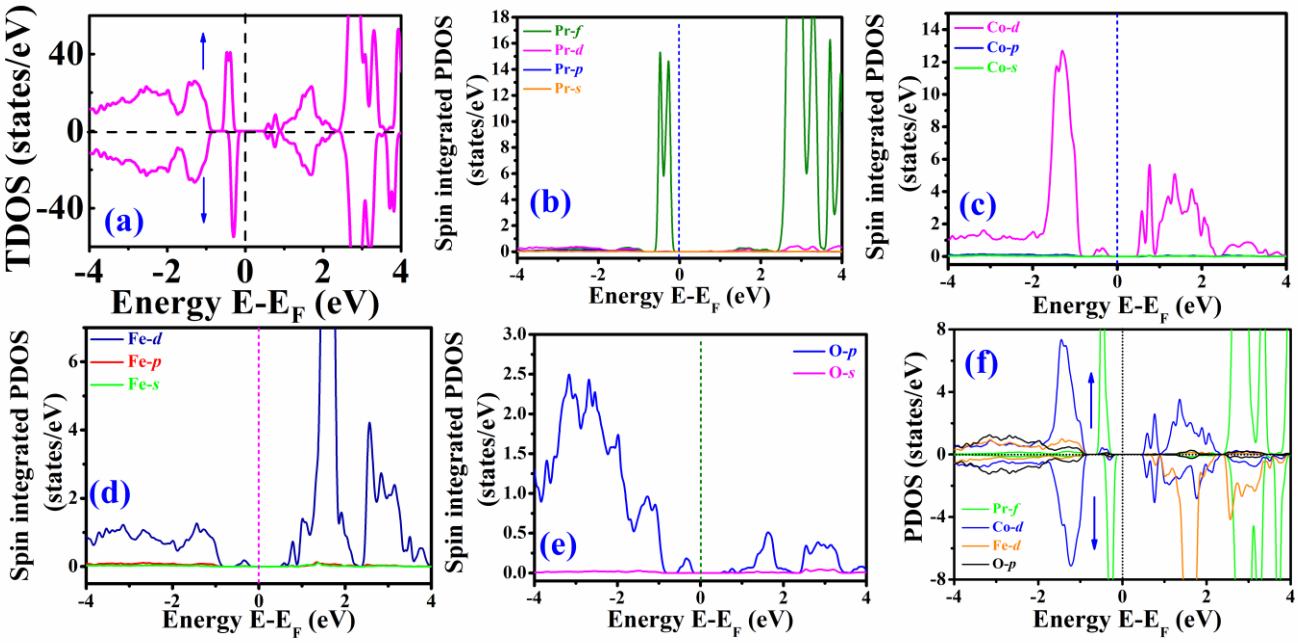

Figure. 6.1: *(a) shows the TDOS as a function of energy (scaled with Fermi energy) for PCFO with AFM coupling in Fe spins. (b), (c), (d) and (e) are depicting the spin integrated PDOS of Pr (s,p,d and f), Co (s,p, and d), Fe (s, p and d) and O (s and p) for PCFO respectively. (f) Shows the spin resolved PDOS for Pr-f, Co-d, Fe-d, O-p orbitals.*

confirmed the systems insulating behaviour. Thus the TDOS calculation corroborates with the experimental results.

Figure. 6.1(b-e) are showing the up and down spin integrated PDOS for Pr-*s/p/d/f*, Co-*s/p/d*, Fe-*s/p/d* and O-*s/p* states. It is evident from Fig. 6.1(b-e) that Pr-*f*, Co-*d*, Fe-*d* and O-*p* states have the dominant contribution in their respective PDOS. No finite DOS is available near the Fermi level for none of the calculated PDOSs, thus confirming the insulating nature of the system. A large splitting can be observed in Pr-*f* PDOS spectra which leads to large energy gap between the unoccupied and occupied states. This large splitting also indicates that the Pr-f electrons are highly localized. Eventually, the large energy gap in Pr-*f* states strongly affects the Co/Fe-*3d* and O-*2p* states. These Co/Fe-*3d* and O-*2p* states get adapted by Pr-*4f* symmetry and hence PDOS related to these states appear in the same energy range as that of Pr-*4f* PDOS. Fig. 6.1(f) is showing the PDOS in both the spin channels for Pr-*f*, Co-*d*, Fe-*d* and O-*p* states. It is clear from the PDOS curves that there is significant hybridization among Co/Fe-*3d* and O-*2p* states. The asymmetric nature in the spin resolved PDOS of Fe-*3d* states clearly suggests its magnetic contribution in its ground state, yielding magnetic moment of 4.43 μ_B for Fe. However, very small spin polarization observed for Co-*3d* (~0.23 μ_B) and O-*2p* is due to strong hybridization with Fe-*3d* and Pr-*4f* states. Thus, the calculations suggests for HS Fe^{3+} ions and LS Co^{3+} ions.

6.4.2 Neutron Diffraction Study:

To get an insight into the microscopic spin arrangement as well as structural order in PCFO, we have undertaken neutron powder diffraction (NPD) study at different temperatures from 300 K down to 6 K. Eventually, the large difference in the coherent neutron scattering lengths of Co (2.49 fm) and Fe (9.45 fm) allows us to probe the degree of B-site ordering in the system which makes the NPD study advantageous over XRD study. The neutron thermo-diffractograms at 300 K and 6 K along with its Rietveld refinements are shown in Fig. 6.2(a-b).

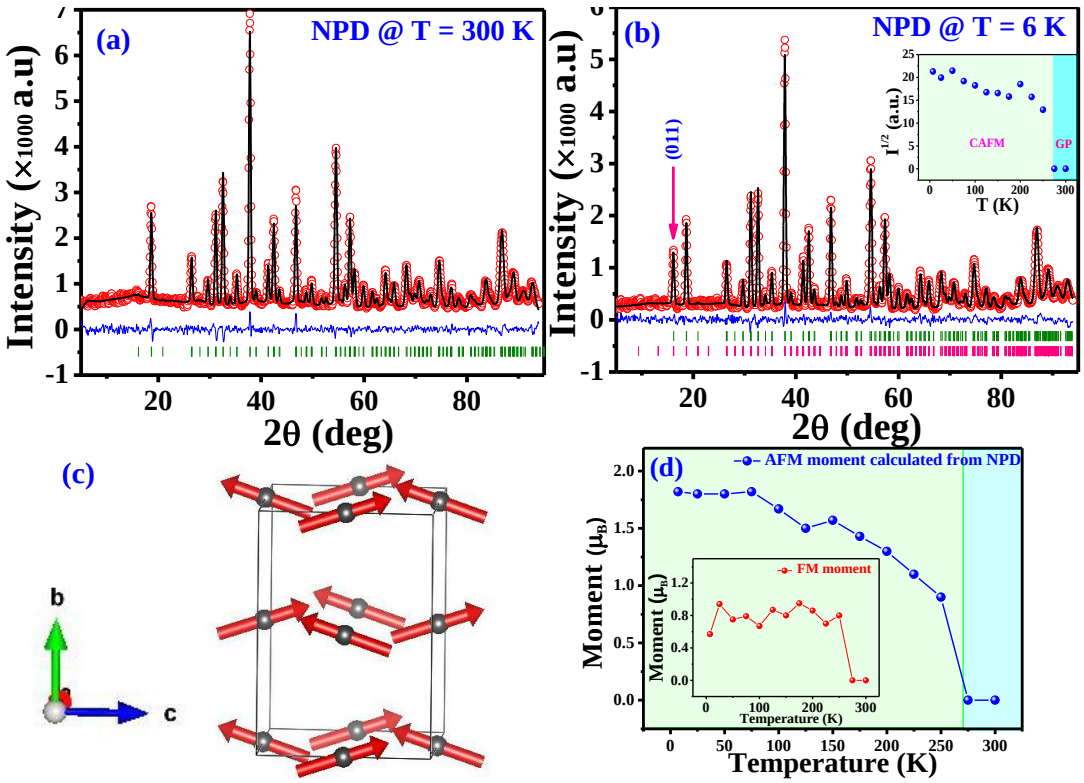

Figure. 6.2: *(a) and (b) show the NPD data @300 K and @6 K with its Rietveld refinements respectively. Inset of Fig. (b) shows the temperature variation of magnetic reflection intensity (c) Depicts the spin ordering obtained from NPD data. (d): Temperature variation of AFM moment while the inset shows that for FM moment calculated from NPD data.*

The refinement of 300 K data was done only with nuclear phase Pnma whereas 6 K data was refined by considering both the nuclear phase (Pnma) and magnetic phase with P-1 space-group. The refinement suggests that the compound crystallizes in B-site disordered single phase orthorhombic structure with Pnma symmetry which is isostructural to its end members i.e. $PrCoO_3$ and $PrFeO_3$. Andersen et. al. have investigated the effects of same charge state of B-site ions on its structure [50]. One of its important aspects is that the structure becomes centro-symmetric due to the random site distribution of B-site ions. The refinement suggests that PCFO sample also crystallizes in a centro-symmetric orthorhombic structure with Glazer notation $a^+a^-b^-$ tilt system, thus indicating same charge states for Co/Fe

ions [51]. The calculated structural parameters such as lattice parameters (a,b,c and angles α, β, γ), atomic positions, bond lengths and bond angles are summarized in Table 6.1. For, PCFO system, the deviation from cubic to orthorhombic structure is triggered by the small size of A-site ion. However, the distortion of octahedra: Co(or Fe)O_6 can simply be measured by the formula $\delta=(180^0-\varphi)/2$, where the φ is a measure of angle Co(Fe)-O-Co(Fe) [52]. From Table 6.1 the reduced bond angle of Co(Fe)-O1-Co(Fe) is found to be 159.03^0 (at 300 K), hence the sizeable distortion found for PCFO is $\delta\sim10.49^0$. Apart from this, the ionic radii for Fe^{3+} (H.S), Co^{3+} (LS) and O^{2-} are 0.645 Å , 0.545 Å, 1.38 Å respectively, hence simply by summing up their ionic radii and taking the mean, we get the average theoretical bond-length Fe/Co-O to be 1.97 Å [53]. Now, from the NPD data (300 K) analysis, it can be seen from Table 6.1 that values of bond lengths Fe/Co-O1, Fe/Co-O21 and Fe/Co-O22 are 1.9538 Å, 1.979 Å and 1.958Å respectively. Thus the estimated bond lengths show a close match with the theoretical bond length for Fe^{3+} (HS) and Co^{3+}(LS) ions. On the other hand, for Co^{3+}(HS) and Fe^{3+} (H.S), the theoretical average bond length of Fe/Co-O is 2.01 Å which does not match with any of the experimentally obtained Fe/Co-O bond lengths. Thus, the analysis suggests a low spin state of the Co^{3+} (LS).

Table 6.1: Structural parameters and crystallographic sites determined from Rietveld refinement of the NPD data at 300 K and 6 K.

Space group: Pnma

Temperature	300 K	6 K
a (Å)	5.4517(6)	5.4513
b (Å)	7.6847(9)	7.6737
c (Å)	5.4365(8)	5.4278
V ($Å^3$)	227.7605	227.0538
Pr	4c	4c
x	-0.0366(10)	-0.0358(9)
y	0.25000	0.25000
z	-0.0088(19)	-0.0144(17)
B_{iso} ($Å^2$)	0.51(8)	0.22(8)
Co/Fe	4b	4b
x	0.00000	0.00000
y	0.00000	0.00000
z	0.50000	0.50000
B_{iso} ($Å^2$)	0.21	0.21
O1	4c	4c
x	0.5130(11)	0.5151(9)
y	0.25000	0.25000
z	0.0641(16)	0.0541(10)
B_{iso} ($Å^2$)	1.06(11)	0.77(9)
O2	8d	8d
x	0.2860(8)	0.2905(6)
y	-0.0408(6)	-0.0458(5)
z	0.2835(8)	0.2855(6)
B_{iso} ($Å^2$)	0.85(5)	0.58(5)
$d_{Co\text{-}O(1)}$/ $d_{Fe\text{-}O(1)}$ (Å)	1.9538(16)	1.9442(8)
$d_{Co/Fe\text{-}O21}$ (Å)	1.979	1.995
$d_{Co/Fe\text{-}O22}$ (Å)	1.958	1.96
<(Fe)-(O1)-(Fe)> or <(Co)-(O1)-(Co)>(deg)	159.03	161.33
<(Fe)-(O2)-(Fe)> or <(Co)-(O2)-(Co)>(deg)	155.83	153.11

Moreover, the NPD pattern analysis with P-1 symmetry yielded a G_zF_y type of spin ordering which is a canted AFM type of magnetic structure. In this structure, the FM moment is directed along y direction while the G-type of magnetic ordering is occurring along z-direction. The microscopic spin arrangements in the G_zF_y magnetic structure is shown by a schematic diagram in Fig. 6.2(c). The magnetic moment analysis from NPD pattern at 6 K gives the moment values 1.82 μ_B and 0.6 μ_B from the AFM and FM contributions respectively. Thus, it predicts a dominating AFM with weak FM ordering. Fig. 6.2(d) and its inset are showing the temperature variation of the AFM and FM moments obtained from the NPD refinements respectively. Both the curves are exhibiting a drastic jump below 275 K, indicating a second order magnetic phase transition near this temperature. As a matter of fact, below 275 K, the calculated total moments for the present magnetic structureare found to be

in the range of ~1.5-2 μ_B, which are comparable to the theoretically expected average saturated moment ~2.5 μ_B for Co^{3+}(LS) and Fe^{3+} (HS) ions. In the contrary, for Co^{3+} (HS) and Fe^{3+}(HS) ions, the theoretically predicted total moment is 4.5 μ_B which is much higher value than our experimentally obtained values. Thus, the analysis confirms the low spin state (LS) for the Co^{3+} ions.

Interestingly, NPD data recorded at 6 K shows an intense super-lattice reflection peak (011) at ~16^0 which was merely absent at 300 K (Fig. 6.2(a-b)). The nuclear contribution to this reflection (011) is absent or minimal while it has significant contribution from magnetic phase P-1. The inset of Fig. 6.2(b) is showing the variation of the intensity of this magnetic reflection with temperature. It is evident that the magnetic reflection gained intensity dramatically below 275 K, thus suggesting establishment of long range magnetic ordering below this temperature. It is relevant to mention here that similar systems have also shown such G-type of canted AFM spin ordering [54-56].

6.4.3 Magnetization Study:

The temperature (T) variation of magnetization (M) of PCFO following the standard zero-field cooled (ZFC) and field cooled (FC) protocols at an applied dc field of 250 Oe, has been illustrated in Fig. 6.3(a). The magnetization curve displays a sharp jump below T_N ~269 K, thus suggesting a second order magnetic phase transition and agreeing to the similar result observed in NPD data. The exact transition temperature is identified from the inflection point of temperature dependent (dM/dT) curve at 269 K (Fig. 6.3b). To further probe the nature of the magnetic transition, we have recorded the ac susceptibility around this temperature (Fig. 6.3c). The sharp and frequency independent ac χ' peaks at ~ 269 K confirm the long range magnetic ordering [11]. Interestingly, at lower temperature ~25 K, another relatively broad anomaly is observed in dM/dT, which is an indication of existence of another magnetic phase

at low temperatures. The FC and ZFC arms show a thermo-magnetic irreversibility or bifurcation below T_N ~269 K, suggesting existence of competition between different magnetic interactions or spin frustrations.

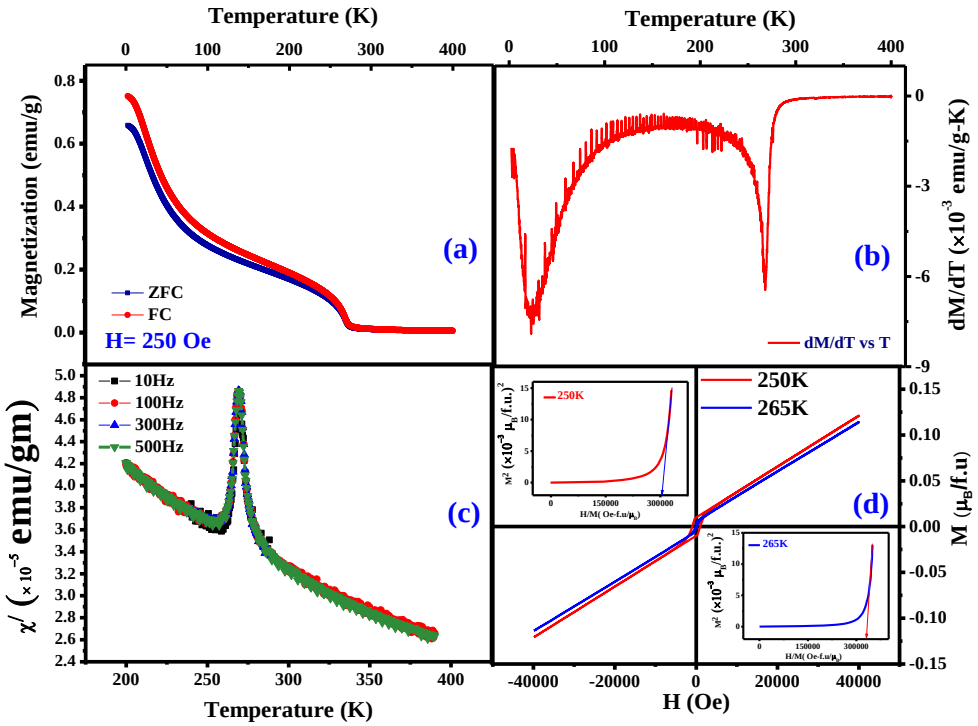

Figure. 6.3: *(a): ZFC and FC M(T) curves recorded at H=250 Oe. (b) shows the "dM/dT Vs T" plot @H=250 Oe. (c): Temperature variation of ac χ' (real) at different frequencies. (d): M(H) curves recorded at 265 K and 250 K. The inset top and bottom show the "Arrot plot" of the M(H) curves at 250 K and 265 K respectively.*

Further investigations have been done by recording the isothermal field variation of magnetization (M-H) near T_N i.e. at 265 K and 250 K (Fig. 6.3d). For both the curves, existence of small hysteresis can be discernible. The exhibition of hysteretic nature with the

coercive field of the M(H) loops is a characteristic of common ferromagnetic (FM) or ferrimagnetic (FIM) materials due to blocking of the domain wall motion. However, no signature of magnetic moment saturation can be seen even at such a high field of 40 KOe, rather it increases monotonically yielding a magnetic moment of $0.12\mu_B$/f.u. (at 250 K) thus indicating predominant canted AFM spin ordering in PCFO. AFM nature of the sample can be attributed to the anti-parallel alignment of Fe^{3+} spins due to AFM Fe^{3+}-O^{2-}-Fe^{3+} exchange interactions. The weak ferromagnetism rises due to the canting of Fe^{3+} spins which can be elucidated by the Dzyaloshinsky-Moriya interaction [57-58]. Apart from this, Co^{3+} ions do not play any role in the exchange interactions as these are in non-magnetic LS state. For further investigations, the virgin curves of the M(H) loops are used in Arrot plot : M^2 Vs H/M at temperatures 265 K and 250 K (inset of Fig. 6.3(d)) [59]. We obtain a negative intercepton the M^2 axis by making a linear extrapolation to H→0 Oe of the higher field portion of the Arrot plot which confirms the absence of spontaneous magnetization below the transition temperature. This clearly suggests the dominating AFM nature of the sample. Additionally, according to Banerjee's theory, the observation of the positive slope of the Arrot curves in our case confirms the second order phase transition occurring at T_N ~269 K [60].

Most interestingly, in the "temperature variation of inverse susceptibility χ^{-1} (T)" curves (Fig. 6.4) at different applied fields ranging from 250 Oe to 3 T, a rapid down-turn deviation from CW behaviour occurs at temperatures well-above the magnetic ordering temperature (T_N ~269 K). This feature is a hallmark for a special magnetic phase known as Griffiths phase (GP) where the system neither behaves like a paramagnet nor shows long range ordering [20-27]. This phase evolves due to the nucleation of finite sized correlated regions or/and clusters having short range magnetic ordering embedded in the global paramagnetic matrix above magnetic transition temperature. On increasing magnetic field, the down turn behaviour is observed to get softened and with sufficiently high field, it yields

CW like behaviour, which is also a characteristic for GP [Fig. 6.4]. Most interestingly, in the "temperature variation of inverse susceptibility χ^{-1} (T)" curves (Fig. 6.4) at different applied fields ranging from 250 Oe to 3 T, a rapid down-turn deviation from CW behaviour occurs at temperatures well-above the magnetic ordering temperature (T_N ~269 K). This feature is a hallmark for a special magnetic phase known as Griffiths phase (GP) where the system neither behaves like a paramagnet nor shows long range ordering (i.e. singularities occur in the thermodynamic properties viz., magnetization etc) [20-27]. This phase evolves due to the nucleation of finite sized correlated regions or/and clusters having short range magnetic ordering embedded in the global paramagnetic matrix above magnetic transition temperature. On increasing magnetic field, the down turn behaviour is observed to get softened and with sufficiently high field, it yields CW like behaviour, which is also a characteristic for GP [Fig. 6.4].

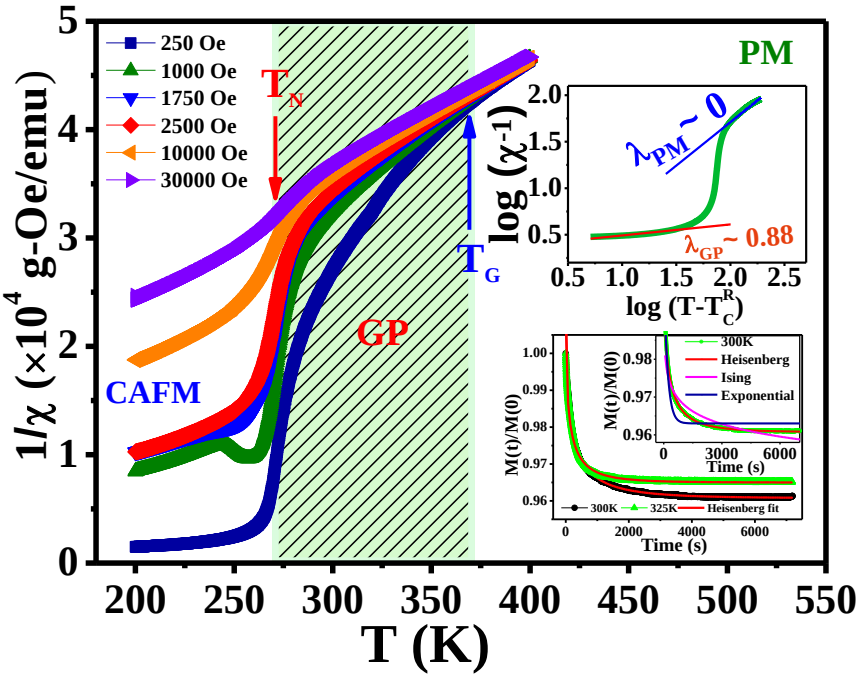

Figure. 6.4: *"χ^{-1} Vs T " plot at different magnetic fields (H) have been shown. Inset top is showing the "log_{10}-log_{10}" plot of "χ^{-1} Vs ($T-T_c^R$). Inset bottom shows the TRM study at 300 K and 325 K and its Heisenberg fit. The inset shows the Heisenberg, Ising and exponential fit of TRM data at 300 K.*

In GP regime, magnetisation doesn't follow CW law rather it follows the power law of inverse susceptibility with a characteristic non-universal exponent λ describing Griffiths singularity [22];

$$\chi^{-1}(T) \propto (T-T_c^R)^{1-\lambda}, (0<\lambda<1)$$

Here, the parameter λ is a measure of deviation from CW behaviour and T_c^R is the magnetic transition temperature of diluted system [20,21]. To further investigate the result, we have fitted our inverse susceptibility curve at H=250 Oe with the above formula. The GP temperature is estimated to be T_G~ 370 K below of which the down-turn behaviour is observed violating the CW law. Now, in above formula, value of T_c^R is so chosen that the fitting in the paramagnetic region above T_G, yields λ_{PM} ~ 0, which is the same procedure as followed by Pramanik et al [23]. The inset (top) of Fig. 6.4, showing the $\log_{10}$-$\log_{10}$ plot of χ^{-1} Vs ($T-T_c^R$), where the linear fitting in the GP region ($T<T_G$) gave the value of λ ~ 0.88 which confirmed the existence of Griffiths phase in PCFO.

However, the spin dynamics in the correlated GP region is expected to be slower than that in PM region. Bray argued that the spin dynamics in the GP region does not follow the exponential decay unlike in the PM region. Therefore, he used two models for interacting spins, namely Heisenberg model and Ising model, for investigating the spin dynamics in the GP region [61]. For the diluted rare magnetic region (GP), he defined a spin auto-correlation function C(t) of the form:

$C(t) \propto \exp\left(-A\left(lnt^{\frac{d}{d-1}}\right)\right)$: For Ising system

$C(t) \propto \exp(-Bt^{1/2})$: For Heisenberg System

Therefore, we have carried out time variation of isothermal remanant magnetization (TRM) measurements of PCFO in the GP regime for further confirmation of GP. A field cooling of the sample with H=1 T is done from 400 K to the desired temperature in GP. The IRM data was recorded after sudden removal of the field by measuring the residual magnetization at 300 K and 325 K as a function of time (bottom inset of Fig. 6.4). The data was not fitted with exponential power law, thus ruling out the existence of pure PM phase above T_N (sub-inset bottom of Fig. 6.4) [62]. However, it is observed that the TRM curve is best fitted for a decay scheme with C(t) defined for Heisenberg spin model while it deviates both from exponential as well as Ising model decay schemes. Thus, the spin interactions in PCFO seem to be following Heisenberg spin model. Again, it suggests the slowing down of the spin dynamics which is expected in a correlated region with short range magnetic ordering, thus confirming the existence of GP in PCFO.

However, to elucidate the origin of the observed GP in PCFO, we may consider the role of the B-site disorder as it was reported to play major role in the evolution of GP in other systems [23,63]. In the pioneering work published by Imry and Ma, the random quenched disorder has been reported to hinder the formation of long range magnetic ordering while favouring the nucleation of correlated clusters [64]. Thereafter, quenched disorder is a key factor for producing GP in many systems [22-23,64-68]. Thus, the quenched disorder in the form of B-site disorder giving rise to random exchange bonds is a potential source of Griffiths singularities. For PCFO, the random distribution of non-magnetic LS Co^{3+} and magnetic Fe^{3+} ions at B-sites give rise to random non-magnetic dilution of Fe^{3+} spins. This forms the perfect platform for percolating correlated clusters in PM matrix, thus triggering the formation of GP in the system. Additionally, the spin canting due to DM interactions introduces the competitive AFM/FM interactions which together with the B-site disorder creates random exchange bonds (not only by values but also by their signs), thus leaving the

system frustrated which is also responsible for the formation of correlated clusters in the PM matrix, thus the GP. It would be pertinent to mention that a very recent report on a very similar DP Pr_2CrFeO_6, no magnetic long range ordering (thus Griffiths phase is not relevant here) was observed, where both Cr^{3+} and Fe^{3+} are in high spin state [36]. The manifestation of such different behaviours by two such similar systems, undoubtedly suggests that the nonmagnetic LS state of Co^{3+} is playing a crucial role in emerging the GP in PCFO. Though, the B-site disorder does not cause any structural distortions or the strains in the system due to the equivalent ionic radii of $Co^{3+}$and Fe^{3+} ions. Thus, such structural distortions or strain mediated enhancement of GP can be ruled out. On the other hand, Desisenhofer et al argued that static quenched disorder introduced by Jahn-teller (J-T) distortion is responsible for the emergence of GP in $La_{1-x}Sr_xMnO_3$ [65]. However, for PCFO, the GP is not associated to J-T effect as neither Fe^{3+}(HS) nor Co^{3+}(LS) exhibit J-T effect. Further, in the contradistinction, Salaman et al have explained the onset of GP in $La_{1-x}Ca_xMnO_3$ ($x\rightarrow 0.3$) due to the structural distortion driven bending of Mn-O-Mn bond angle causing alterations in the exchange interactions [22]. Thus the observed octahedral distortion of FeO_6 octahedra in PCFO causing the concurrent changes in the Fe^{3+}-O-Fe^{3+} exchange interactionsmay also play an important role in the evolution of GP by aiding the cluster formation in the PM matrix. However, irrespective of all the above situations, B-site disorder together with non-magnetic Co^{3+} (LS) ions producing random exchange bonds seem to be the main plausible origin for the observed GP in PCFO. Eventually the observation of GP in AFM based PCFO system is amongst the rare findings and thus indicates the need for more theoretical and experimental studies on such AFM systems to shed new light in to the understanding of such unconventional GP behaviour.

Apart from this, we reiterate that the dc ZFC and FC magnetization curves showed a sudden slope change at low temperatures (dM/dT showed anomaly near ~25 K) suggesting

presence of a secondary phase at lower temperatures. In contrast to the dc magnetization study, ac susceptibility measurements can probe the spin dynamics of a system and thus we have carried out these measurements in our system [69]. Figure. 6.5(a) and its inset are showing the temperature variation of imaginary χ'' and real χ' parts of ac susceptibility data. The curves $\chi'(T)$ show clear anomaly below 40 K which on increasing frequency becomes more prominent, thus suggesting a slow spin relaxation process. The corresponding Kramers-Kronig peaks in χ''(T) are clearly observed near ~ 34 K which exhibit strong frequency dependence of its peak positions: a typical feature of spin glass (SG) state (Fig. 6.5(a)) [28-29,69-70]. Again, these new peaks are quite broad extending over a temperature interval of ~70 K (unlike the λ-like sharp long range ordering peaks) which also suggests it to be a glassy transition [11,70]. Thus, noting all these characteristic features, it is comprehensible that the present system enters in a re-entrant spin-glass (RSG) like state at low temperatures (<40 K).

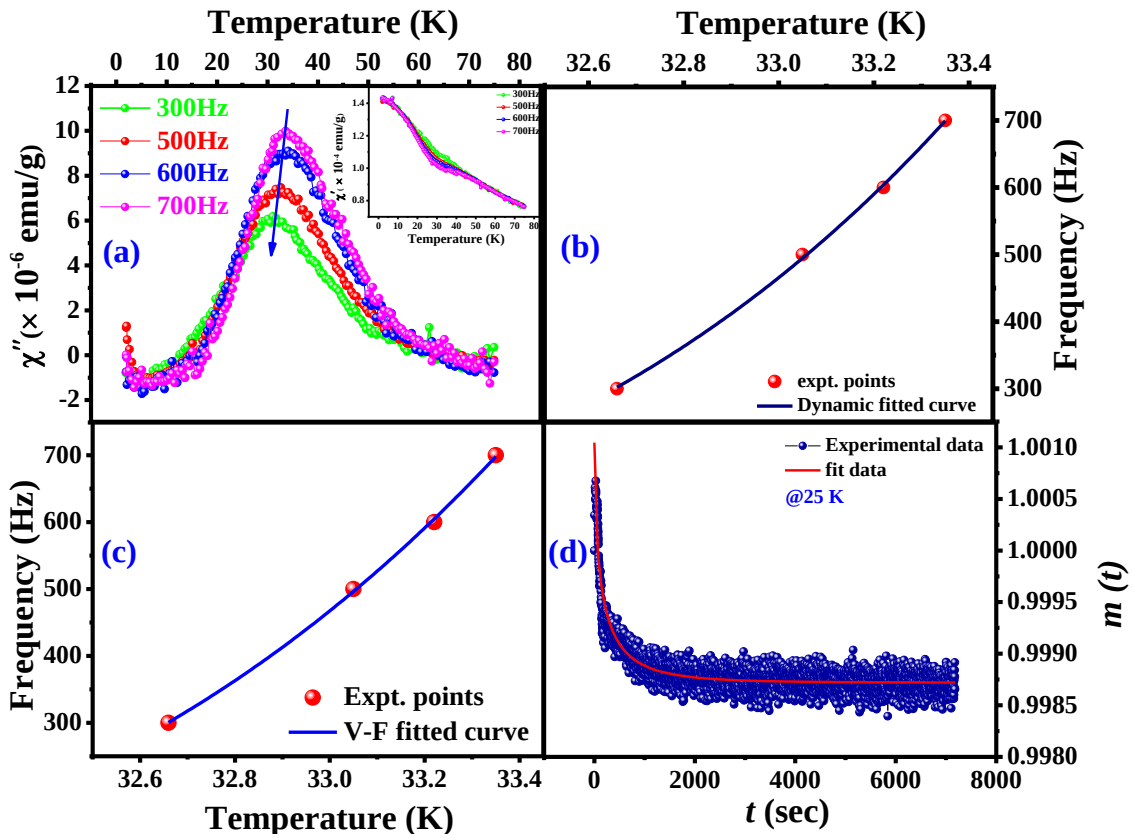

Figure. 6.5: *(a): "χ'' Vs T" curves at different frequencies are shown. Inset showing the corresponding $\chi'(T)$ curves. Fig. (b) and (c) are showing the dynamic fit and Vogel-Fulcher fit of the T_f (T) data. (d): KWW stretched exponential equation fit of the TRM curve at 25 K.*

For getting further insights into RSG state, we have fitted the data in different models. From the frequency dependence of the ac peaks, we have calculated Mydosh parameter (p) which is a universal tool to distinguish SG state [70]. Here,

$$p = \frac{\Delta T_f}{T_f \Delta log_{10}(f)},$$

Where $\Delta T_f = T_{f1} - T_{f2}$ and $\Delta log_{10}(f) = log_{10}(f1) - log_{10}(f2)$. For, typical SG or CG systems, p lies between 0.005 and 0.08, while for super paramagnetic system, it is greater than 0.2. The obtained value of p ~ 0.05 for PCFO confirms the glass type state.

Moreover, in a SG or CG state, the spin dynamics gets slowed down below the critical temperatures T_f. This critical slowing down of spins near T_f, can be investigated using the dynamic scaling law [29,71]

$$f = f_0 \left(\frac{T_f - T_{SG}}{T_{SG}}\right)^{z\nu} ;$$

Where the f is the excitation frequency, T_{SG} is the equivalent spin glass freezing temperature in the limit of $f \rightarrow 0\ Hz$ *and* $H_{DC} \rightarrow 0\ Oe$, f_0 is related to the characteristic spin flipping time (τ_0) as $f_0 = \frac{1}{\tau_0}$; zν is the dynamical critical exponent. In Fig. 6.5(b), "f Vs T_f" curve has been plotted and the best fitting with the above dynamical scaling law yielded: $f_0 \sim 6\times10^6$ Hz ($\tau_0 = 1.67\times10^{-7}$ s), T_{SG} = 29 K (which is near to the observed spin glass freezing temperatures) and the exponent zν is found to be ~ 4.6 which is satisfactory for spin glass state ($4 < z\nu < 12$). For a canonical SG system, τ_0 typically lies between ~ 10^{-12}-10^{-13} s which is less than the observed value ~10^{-7} s by few orders. The larger spin flipping time is suggesting the observed transition is due to freezing of finite sized clusters (which take more time to relax) rather than individual spins [29,71].

For further investigations of inter-cluster interactions, the empirical Vogel-Fulcher (VF) law can be employed to fit the above curve "f *vs* T_f". The law being of the form [29]:

$$f = f_0 \exp\left(-\frac{E_A}{K_B(T_f - T_0)}\right);$$

Where f_0 is a characteristic frequency, T_0 is formally known as VF parameter which is a temperature representing the strength of inter-cluster interaction strength and E_A is the activation energy. Figure. 6.5(c) shows the fitted graph using the V-F law. The best fitting yielded $f_0 \sim 10^6$ Hz (which is of the same order of f obtained from previous dynamic scale fitting), T_0=27.45 K and E_A/K_B=37.4 K. The comparable values of T_0 and activation energy indicate existence of strong inter-cluster couplings in the system. The obtained large value of $\tau_0 = \frac{1}{f_0}$ is again suggesting the presence of interacting magnetic spin clusters.

Another experimental realization of slow spin relaxation in the SG or CG state can be found in the "time (t) evolution of remanent magnetization m(t) (TRM)" below T_f. The measurement was carried out following field cooled (FC) protocol. The sample was cooled with a field H=0.1 T down to 25 K (below T_f) and the TRM data was recorded after switching off the magnetic field. The normalized magnetization m(t)=$\left(\frac{M_t}{M_{t=0}}\right)$ has been plotted as a function of time and shown in Fig. 6.5(d). The TRM data can be analyzed using KWW (Kohlrausch Williams Watt) stretched exponential equation as given below [72]:

$$m(t) = m_0 - m_g exp\left\{-\left(\frac{t}{\tau}\right)^{\beta}\right\};$$

Here, m_0 is associated to the initial remanent magnetization, m_g is representing the magnetization of glassy component, τ is the characteristic relaxation time constant and β is the shape parameter or stretching exponent. Another power law also often used for the analysis of TRM data is m(t) $\propto t^{\pm\alpha}$[72]. However, we tried to fit our TRM data with both the above relations but found that the best fitting is obtained with the KWW model, shown in Fig 6.5(d). The fitting was not satisfactory for the power law ($t^{\pm\alpha}$), and not shown here. The KWW fitting is a powerful technique which is widely used for the investigations of the m(t) data for glassy or disordered systems [72]. For different class of disordered systems, the β value lies in between 0 and 1. The obtained β value for PCFO is ~ 0.52, thus confirming the existence of glassy state at this temperature (25 K).It is relevant here to note that even below the freezing temperature T_f ~34 K, the long range magnetic ordering still exists (as evident from NPD data) which occurs for a re-entrant spin or cluster glass systems. Therefore, all the above facts confirm the system entering in a RCG state at low temperatures. Present system PCFO contains the two major microscopic ingredients for glassy transitions: (i) B-site disorder and (ii) Spin canting [11,30,73]. In pure FM or AFM systems, the domain formation involves microscopic time scales but due to the presence of disorder, it causes pinning of the

domain wall which essentially gives rise to metastable states. It does not allow the system to attain an equilibrium state in the experimental time scale leading to non-equilibrium phases like spin-relaxations, aging effects etc [31,73]. In PCFO, the B-site disorder causes the local environment of the magnetic spins (Fe^{3+}) to be inhomogeneous. Thus it leads to the formation of random exchange bonds causing the spin frustration which at low temperatures ends up in random, non-collinear, frozen states of spins leading to RCG state. Again, the spin canting is also an important and potential ingredient for glassy sate which can eventually cause random partial freezing at lower temperatures of the existing sets of non-collinear ferromagnetically or antiferromagnetically coupled spins; thus leading to the RSG or RCG states [30,74]. Hence for PCFO, the high temperature (T_N ~ 269 K) long range ordered canted AFM state gets frustrated due to the increasing competition of AFM and FM interactions with lowering temperature, thus reaching to a RCG state. Eventually, a RCG state evolves when one of the competing interactions dominates the other unlike the RSG state where both FM/AFM states are of equal order [29,30]. Thus, the dominating AFM interaction in PCFO is presumably associated to the observation of the RCG state.

To further investigate the evolution of the different magnetic states; we have recorded M-H loops at different temperatures as shown in Fig. 6.6(a)(1-4). It can be noted that the magnetic hysteresis loop has been enhanced appreciably as temperature is cooled down to 200 K, suggesting effective increase in FM contribution (Fig. 6.6a(1-2)). However, as temperature is further decreased to 125 K, surprisingly the squareness of the loop (FM feature) got diminished (Fig. 6.6a(3)). This may be a prior indication that the system is entering in a glassy state. Moreover, the presence of competing FM/AFM interactions is evident from the M-H curves. Eventually, similar changes in the shapes of the M-H loops were observed in an orthoferrite $SmFeO_3$ [75]. We can reiterate here thatin dc ZFC and FC a slope change forming a smeared hump below 10 K was observed (Fig. 6.3(a)). Similarly, in

the NPD data, the FM moment dropped to its lowest value (0.57 μ_B) at 6 K (inset of Fig. 6.2(d)). All these three observations are seemingly associated to the onset of polarization of the paramagnetic Pr^{3+} moments by the internal field of Fe-spin sublattice [35,75]. Paramagnetic Pr^{3+} moments tend to align anti-parallel to the weak FM component of the Fe-sublattice and cause appreciable compensation in the FM susceptibility. On lowering the temperature, the Pr^{3+} moments get more aligned and lead to the above changes in the magnetization behaviours.

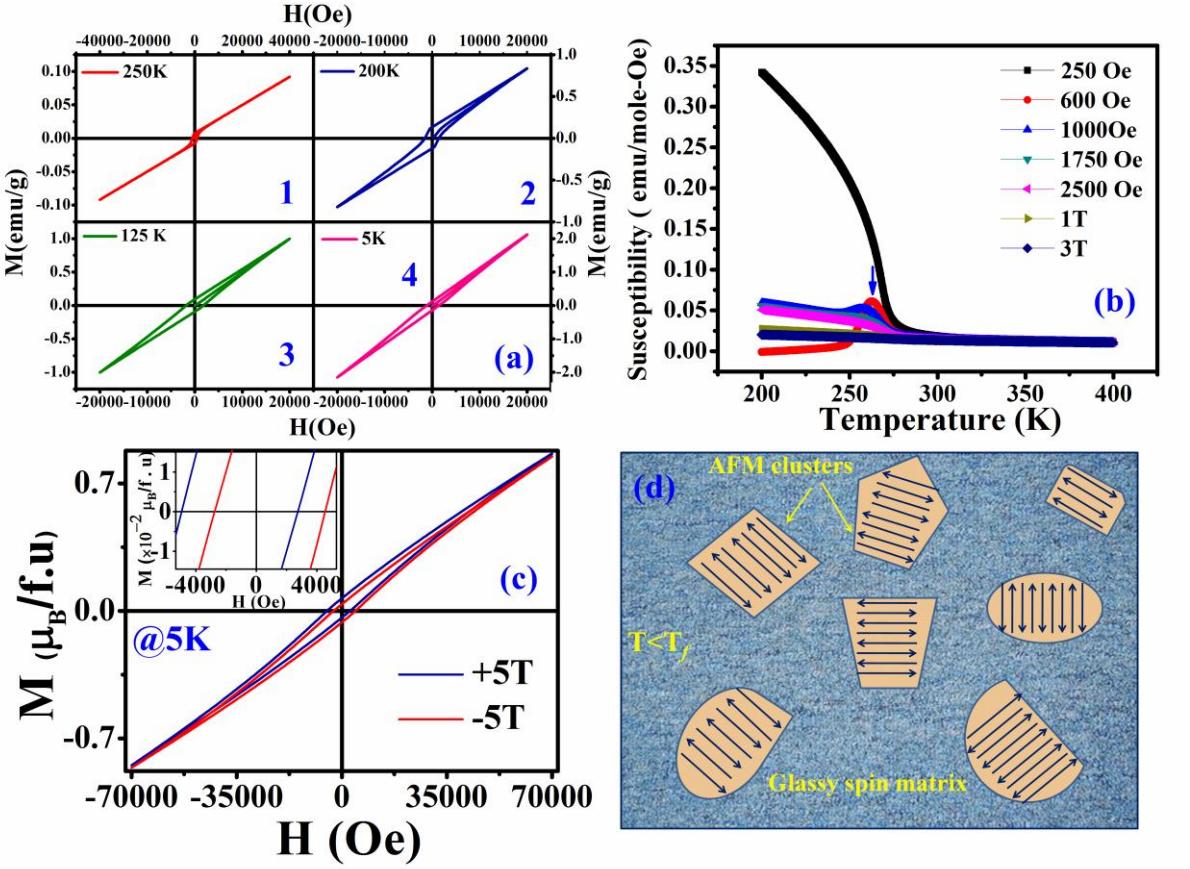

Figure. 6.6: *(a) M(H) curves recorded at different temperatures. (b): Field dependent ZFC M(T) curves. (c) M(H) curves at 5 K recorded after field cooling under H=+/-5 T. (d):The model showing the AFM clusters embedded in a global glassy matrix which gives rise to the exchange bias effect.*

Apart from this, an interesting field induced meta-magnetic behaviour is observed in the ZFC M(T) curves under different fields. As evident from Fig. 6.6(b), the magnetization shows monotonous increase with lowering temperature for moderate field H=250 Oe. Surprisingly, for an increased field 600Oe, it showed a dramatic drop forming a peak below T_N. However, with further increase in fields (e.g. 1000 Oe etc.) the peak gets flattened and gradually disappears with sufficiently high fields (>1 T). To elucidate this observation, we may recall the presence of two Fe sub-lattices (up and down) forming AFM spin configuration. The field and temperature dependences of these two spin sub-lattices are different due to presence of anisotropy of the system and as a consequence for a moderate field, the magnetization rises due to the uncompensated FM moment of the system. On increasing the field, the moments of the two Fe spin sub-lattices cancel each other below T_N and M(T) exhibits the typical AFM peak. However, as the field is increased further, Fe^{3+} spins tend to align along the field, thus fading the peak away which is a common feature of AFM systems [6].

Moreover, meticulous theoretical and experimental studies have revealed that exchange anisotropy across the interfaces of different inhomogeneous magnetic phases such as FM/AFM, FM/Spin glass, FM/Ferrimagnet, hard/soft phases of FM systems are responsible for the observation of exchange bias (EB) effect [76-78]. Hence, knowing the fact that PCFO holds multiple magnetic phases, we got motivated to investigate the EB effect in this system. The conventional EB experiment was performed by cooling the sample in a magnetic field of +/-5 T down to 5 K and recording the M-H loops (Fig. 6.6(c)). Clear evidence of EB effect can be observed from the horizontal shift of the M-H loops. To get quantitative value of EB effect, we have measured the loop asymmetry along the field and magnetization axes as $H_{CEB} = \frac{[H_{c1}-H_{c2}]}{2}$ and $M_{CEB} = \frac{[M_{r1}-M_{r2}]}{2}$ respectively, where H_{C1} and

H_{C2} are the negative or positive intercepts along the field axis of the hysteresis loops recorded with +5 T and -5 T respectively, similarly M_{r1} and M_{r2} are the negative or positive intercepts along the magnetization axis of the said curves. Eventually, we have obtained appreciable values for the above EB parameters: $H_{CEB} \sim 2175$ Oe and $M_{CEB} \sim 0.033$ μ_B/f.u.

The observed EB effect can be elucidated by the co-existence of AFM clusters in the frozen glassy spin matrix [78]. This is demonstrated figuratively in Fig. 6.6 (d). Due to the strong non-switchable unidirectional pinning forces or exchange anisotropy induced at the interfaces of the AFM spin-clusters/glassy spin matrix, the M(H) loop gets shifted exhibiting EB effect [78].

6.5 Conclusion

We have investigated the magnetic properties of a new member of double perovskite Pr_2CoFeO_6 and correlated with its structural and electronic properties. The crucial roles of B-site disorder and spin-state of Co^{3+} have been thoroughly brought out in the evolution of multiple interesting magnetic phases like GP, RCG, meta-magnetic peak and EB effects. The NPD study highlighted the random distribution of Co/Fe ions in the B-site, thus forming a disordered orthorhombic Pnma structure. NPD data analysis also yielded a G-type of AFM spin ordering and it further revealed the spin state of Co^{3+} to be LS. Moreover, ab initio calculations predicted an AFM ground state by showing it is energetically favourable than FM interactions and it also predicted an insulating nature of PCFO. It also predicted a LS non-magnetic state for Co^{3+} ions and HS state for Fe^{3+} ions. Thus, theoretical calculations agreed well with our experimental observations. The B-site disorder present in the system is triggered by the same charge states of B-site ions and this disorder along with the LS Co^{3+} ions effectively created the random non-magnetic dilution of the magnetic Fe spins. As a matter of fact, this random non-magnetic dilution provides the perfect platform for the

preformation of percolating magnetic clusters above T_N ~ 269 K, thus leading to the GP in PCFO. Again, this maidenly recognized GP in AFM PCFO system essentially places it amongst the rare materials which order antiferromagnetically and show features of GP. Additionally, unique to the current system, it showed GP at quite high temperature (269 K<T_G<370 K) range. Spin dynamics study by the ac susceptibility further revealed that the system enters in a RCG state at ~ 34 K where a glassy state is observed to co-exists with global canted-antiferromagnetic state. We found that B-site disorder along with the spin canting driven spin frustration played the major role in bringing out this RCG state in the system. Moreover, the observed low temperature exchange bias (at 5 K) is elucidated through the co-existence of AFM and the glassy states and explained through the AFM core and glassy shell model. The results of the present work can provoke the experimental as well as the theoretical investigations to study the possible impact of such B-site disorder and the spin states on the magnetic properties of different magnetic systems.

References

1. J. Wang, J. B. Neaton, H. Zheng, V. Nagarajan, S. B. Ogale, B. Liu, D.Viehland, V. Vaithyanathan, D. G. Schlom, U. V. Waghmare, N. A. Spaldin, K. M. Rabe, M.Wuttig, and R. Ramesh, Science **299**, 1719 (2003).
2. S.W. Cheong and M. Mostovoy, Nat. Mater. **6**, 13 (2007).
3. Y. Kitagawa, Y. Hiraoka, T. Honda, T. Ishikura, H. Nakamura, and T. Kimura, Nat. Mater. **9**, 797 (2010).
4. F. S. Galasso, Structure, Properties and preparation of Perovskite-type compounds (Pergamon, London, 1969)
5. K.I. Kobayashi, T. Kimura, H. Sawada, K. Terakura and Y. Tokura, Nature,**395**, 677 (1998)
6. G.R. Haripriya, H.S. Nair, R. Pradheesh, S. Rayaprol, V. Siruguri, D. Singh, R. Venkatesh, V. Ganesan, K. Sethupathi, and V. Sankaranarayanan, J. Phys.: Condens. Matter. **29**, 475804 (2017).
7. M.H. Phana, S.B. Tiana , D.Q. Hoanga , S.C. Yua,, C. Nguyenb , A.N. Ulyanov, J. Magn. Magn, Mater. **309**, 258-259 (2003)
8. N.S. Rogado, J. Li, A.W. Sleight, and M.A. Subramanian, Advanced Materials **17**, 2225 (2005).
9. S. Yáñez-Vilar, E.D. Mun, V.S. Zapf, B.G. Ueland, J.S. Gardner, J.D. Thompson, J. Singleton, M. Sánchez-Andújar, J. Mira, N. Biskup, M.A. Señarís-Rodríguez, and C.D. Batista, Phys. Rev. B **84**, (2011).
10. J. Blasco, J. García, G. Subías, J. Stankiewicz, J.A. Rodríguez-Velamazán, C. Ritter, J.L. García-Muñoz, and F. Fauth, Phys. Rev. B **93**, 214401 (2016).
11. D. Choudhury, P. Mandal, R. Mathieu, A. Hazarika, S. Rajan, A. Sundaresan, U.V. Waghmare, R. Knut, O. Karis, P. Nordblad, and D. D. Sarma, Phys. Rev. Lett **108,** 127201 (2012).
12. J. K. Murthy and A. Venimadhav, App. Phys. Lett. **103**, 252410 (2013).

13. H.S. Nair, D. Swain, H. N., S. Adiga, C. Narayana, and S. Elzabeth, J. App. Phys. **110**, 123919 (2011).
14. T. Chakraborty, H. S. Nair, H. Nhalil, K. R. Kumar, A. M. Strydom and S. Elizabeth, J. Phys. Cond. Mater. **29**, 025804 (2017).
15. R. I. Dass and J. B. Goodenough, Phys. Rev B **67**, 014401 (2003).
16. J. B. Goodenough, Phys. Rev. **100**, 564 (1955).
17. M. G. Hernández, J. L. Martínez, M. J. M. Lope, M.T. Casais and J. A. Alonso, Phys. Rev. Lett. **86**, 2443 (2001).
18. A. S. Ogale, S. B. Ogale, R. Ramesh, and T. Venkatesan, App. Phys. Lett. **75**, 537 (1999).
19. G. Sharma, J. Saha, S. D. Kaushik, V. Siruguri, and S. Patnaik, App. Phys. Lett. **103**,012903 (2013).
20. R. B. Griffiths, Phys. Rev. Lett. **23**, 17 (1969).
21. A. J. Bray, M. A. Moore, J. Phys. C **15**, L765 (1982).
22. M. B. Salamon, P. Lin, and S. H. Chun, Phys. Rev. Lett. **88**, 197203 (2002).
23. A. K. Pramanik and A. Banerjee, Phys. Rev. B **81**, 024431 (2010)
24. Z.W. Ouyang, N.M. Xia, Y.Y. Wu, S.S. Sheng, J. Chen, Z.C. Xia, L. Li, and G.H. Rao, Phys. Rev. B **84**, 054435 (2011).
25. A Karmakar, S Majumdar, S Kundu, T K Nath and S Giri, J. Phys.: Condens. Matter **25**, 066006 (2013).
26. K. Ghosh, C. Mazumdar, R. Ranganathan, S. Mukherjee, Sci. Rep. **5**, 15801 (2015).
27. J. Kumar, S. N. Panja, S. Dengre, S. Nair, Phys. Rev. B **95**, 054401 (2017)
28. S. Niidera, S. Abiko, and F. Matsubara, Phys. Rev. B **72**, 214402 (2005).
29. M. D. Mukadam, S. M. Yusuf, P. Sharma, S. K. Kulshreshtha, and G. K. Dey, Phys. Rev. B **72**, 174408 (2005) and references therein.
30. K. Manna, A. K. Bera, M. Jain, S. Elizabeth, S. M. Yusuf, and P. S. Anil Kumar, Phys. Rev B 91, 224420 (2015) and references therein.

31. L. Shlyk, S. Strobel, B. Farmer, L. E. De Long,2, and R. Niewa, Phys. ReV. B **97**, 054426 (2018)
32. S. Ghara, B. G. Jeon, K. Yoo, K. H. Kim, and A. Sundaresan, Phys. Rev. B **90**, 024413 (2014)
33. D. Sherrington and S. Kirkpatrick, Phys. Rev. Lett. **32**, 1792 (1975).
34. M. Gabay and G. Toulouse, Phys. Rev. Lett. **47**, 201 (1981).
35. C. Ganeshraj, R. N. Mahato, D. Divyaa, and P. N. Santhosh, J. Appl. Phys. **107**, 09E305 (2010)
36. N. Das,S. Singh,A. G. Joshi,M. Thirumal, V. R. Reddy, L. C. Gupta, A. K. Ganguli, Inorg. Chem. **56**, 12712 (2017).
37. K. Yoshimatsu, K. Nogami, K. Watarai, K. Horiba, H. Kumigashira, O. Sakata, T. Oshima, and A. Ohtomo, Phys. Rev. B **91**, 054421 (2015).
38. W. M. Xu,1 O. Naaman, G. Kh. Rozenberg, M. P. Pasternak, and R. D. Taylor, Phys. Rev B **64**, 094411 (2001)
39. H. Wu, S. Cao, M. Liu, Y. Cao, B. Kang, J. Zhang, and W. Ren, Phys. Rev. B **90**, 144415 (2014) and references therein.
40. A.H. Bobeck, E. D. Torre, 1975. North-Holl, Amsterdam.
41. Y. S. Didosyan, H. Hauser, G. A. Reider, W. Toriser, J. Appl. Phys. **95**,7339(2004).
42. M. A. Korotin, S. Yu. Ezhov, I. V. Solovyev, and V. I. Anisimov, Phys. Rev. B **54**, 5309 (1996).
43. C. Zobel, M. Kriener, D. Bruns, J. Baier, M. Gru¨ninger, and T. Lorenz, Phys. Rev. B **66**, 020402 (R)(2002).
44. M.W. Haverkort, Z. Hu, J.C. Cezar, T. Burnus, H. Hartmann, M. Reuther, C. Zobel, T. Lorenz, A. Tanaka, N.B. Brookes, H.H. Hsieh, H.-J. Lin, C.T. Chen, and L.H. Tjeng, Phys. Rev. Lett. **97**, 176405 (2006).
45. J. Yu, D. Phelan, and D. Louca, Phys. Rev B **84**, 132410 (2011) and references therein.

46. V.V. Mehta, S. Bose, J.M. Iwata-Harms, E. Arenholz, C. Leighton, and Y. Suzuki, Phys. Rev. B **87**, 020405 (R) (2013).
47. S. K. Pandey, A. Kumar, S. M. Chaudhari and A. V. Pimpale, J. Phys.: Condens. Matter **18**, 1313 (2006)
48. S. K. Pandey, Ashwani Kumar, S. Patil, V. R. R. Medicherla, R. S. Singh, K. Maiti, D. Prabhakaran, A. T. Boothroyd, and A. V. Pimpale, Phys. Rev. B 77, 045123 (2008)
49. Y. L. Lee, J. Kleis, J. Rossmeisl and D. Morgan, Phys. Rev B **80**, 224101 (2009)
50. M. Anderson, K. Greenwood, G. Taylor, and K. Poeppelmeier, Progress in Solid State Chemistry **22**, 197 (1993).
51. A.M. Glazer, ActaCrystallographica Section A **31**, 756 (1975).
52. A. Mu Oz, J.A. Alonso, M.T. Casais, M.J. Mart Nez-Lope, and M.T. Fern N. D Az, J. Phys.: Condens. Matter. **14**, 8817 (2002).
53. R.D. Shannon, Acta Crystallogr., Sect. A **32**, 751 (1976).
54. D. V. Karpinsky, I. O. Troyanchuk, K. Barner, H. Szymczak and M. Tovar, J. Phys.: Condens. Matter **17**,7219 (2005)
55. I. Fita, A. Wisniewski, R. Puzniak, E. E. Zubov, V. Markovich, and G. Gorodetsky,Phys. Rev. B 98, 094421 (2018) and references therein.
56. Y. Wei, H. Gui, Z. Zhao, J. Li, Y. Liu, S. Xin, X. Li, and W. Xie, AIP Adv 4, 127134 (2014)
57. I. Dzyaloshinsky, J. Phys. Chem. Solids **4**, 241 (1958).
58. T. Moriya, Phys. Rev. **120**, 91 (1960).
59. A. Arrott, Phys. Rev. **108**, 1394 (1957).
60. B. K. Banerjee, Phys. Lett. **12**, 16 (1964)
61. A. J. Bray, Phys. Rev. Lett. **60**, 720 (1988).
62. M. Randeria, J. P. Sethna, and R. G. Palmer, Phys. Rev. Lett. **54**, 1321 (1985).
63. J. Fan, L. Pi, Y. He, L. Ling, J. Dai, and Y. Zhang, J. App. Phys. **101**, 123910 (2007).
64. Y. Imry and S. K. Ma, Phys. Rev. Lett. **35**, 1399 (1975).

65. J. Deisenhofer, D. Braak, H.-A. Krug von Nidda, J. Hemberger,R. M. Eremina, V. A. Ivanshin, A. M. Balbashov, G. Jug, A.Loidl, T. Kimura, and Y. Tokura, Phys. Rev. Lett. **95**, 257202 (2005).
66. Y. Shimada, S. Miyasaka, R. Kumai, and Y. Tokura, Phys. Rev. B **73**, 134424 (2006).
67. S. Guo, D. P. Young, R. T. Macaluso, D. A. Browne, N. L. Henderson, J. Y. Chan, L. L. Henry, and J. F. DiTusa, Phys. Rev.Lett. **100**, 017209 (2008).
68. C. Magen, P. A. Algarabel, L. Morellon, J. P. Ara´ujo, C. Ritter,M. R. Ibarra, A. M. Pereira, and J. B. Sousa, Phys. Rev. Lett. **96**,167201 (2006).
69. J. Mydosh, J. Magn. Magn. Mater. **157-158**, 606 (1996).
70. J. A. Mydosh, Spin Glasses: An Experimental Introduction (London: Taylor and Francis), 1933
71. C. Djurberg, P. Svedlindh, P. Nordblad, M. F. Hansen, F. Bødker, and S. Mørup, Phys. Rev. Lett. **79**, 5154 (1997).
72. A. Ito, H. Aruga, E. Torikai, M. Kikuchi, Y. Syono, and H. Takei, Phys. Rev. Lett. **57**, 483 (1986).
73. E. Vincent, V. Dupuis, M. Alba, J. Hammann, and J. P. Bouchaud, Euro. Phys. Lett. **50**, 674 (2000).
74. P. Mahadevan, F. Aryasetiawan, A. Janotti, and T. Sasaki, Phys. Rev. B **80**, 035106 (2009).
75. S. Chaturvedi,P. Shyam, R. Bag, M. M. Shirolkar, J. Kumar, H. Kaur, S. Singh, A. M. Awasthi, and S. Kulkarni, Phys. Rev. B **96**, 024434 (2017)
76. W. H. Meiklejohn and C. P. Bean, Phys. Rev. **102**, 1413 (1956).
77. M. Ali, P. Adie, C.H. Marrows, D. Greig, B.J. Hickey, and R.L. Stamps, Nat. Mater. **6**, 70 (2007).
78. X. K. Zhang, J. J. Yuan, Y. M. Xie, Y. Yu, F. G. Kuang, H. J. Yu, X. R. Zhu, and H. Shen, Phys. Rev. B **97**, 104405 (2018) and references therein.